Electronic Supplementary Material (ESI) for Lab on a Chip.

Electronic Supplementary Information

Intolerance of Profligacy: Aptamer Concentration Gradient-Tailored Unicellular Array for High-Throughput Biologics-Mediated Phenotyping

Xuan Zhang,‡ Ya-Nan Zhao,‡ Xing Wei, Xue Men, Cheng-Xin Wu, Jun-Jie Bai, Ting Yang, Ming-Li Chen,* Jian-Hua Wang*

Research Center for Analytical Sciences, Department of Chemistry, College of Sciences, Northeastern University, Box332, Shenyang 110819, China

Corresponding Author

*E-mail address: chenml@mail.neu.edu.cn. (M.-L. Chen),

jianhuajrz@mail.neu.edu.cn (J.-H. Wang).

Tel: +86 24 83688944.

Experimental

Materials and chemicals.

RTV 615 poly (dimethylsiloxane) (PDMS) pre-polymer and curing agent were purchased from Momentive Performance Materials (Waterford, NY, USA). Surface-oxidized silicon wafers were obtained from Shanghai Xiangjing Electronic Technology, Ltd. (Shanghai, China). SU8-2050 photoresist was provided by MicroChem (Newton, MA, USA). Nitric acid and hydrogen peroxide were the products of Sinopharm Chemical Reagent Co., Ltd (Shanghai, China). Tween 20 was received from Aladdin Reagent Co., Ltd (Shanghai, China). Dulbecco's modified Eagle's medium (DMEM), fetal bovine serum (FBS), trypsin and phosphate buffer solution (PBS) were the products of Gibco Invitrogen Corporation (CA, USA). The analytical reagent-grade solvents and other chemicals were received from the local commercial suppliers, unless otherwise specified. All solutions were prepared using ultra-purified water supplied by a Milli-Q system (Millipore®). HepG2 cells and SK-Hep-1 cells were kindly supplied by Stem Cell Bank, Chinese Academy of Sciences.

Apparatus and imaging analysis

Two syringe pumps (Pump 11 Elite, Harvard, USA) were used for fluidic delivery. An inverted microscope (Olympus, BX53M) with a charge coupled device camera (Olympus, DP74) and a mercury lamp (Olympus, U-RFLT50) were used for cell monitoring and fluorescence observation. The imaging and data analyses were carried out using Image-Pro1 Plus 6.0 (Media Cyternetics, Silver Spring, MD), Image J v1.8.0 (National Institutes of Health), and origin 9.5 (origin Inc.).[1, 2]

Numerical simulations

To evaluate fluid motion, vortex distribution in the microfluidic system, computational fluid dynamics (CFD) simulation was performed using Comsol Multiphysics 5.4 (Comsol) on an eight-core, 64-bit computer (Asus) with 64 GB of RAM. The simulation environment was verified for steady-state incompressible flows in the section of "Dean-like secondary flow acceleration". Different flow rates were specified at the inlet, and the outlet was set to a fixed-pressure boundary condition. No slip boundary condition was applied at the channel walls. Multiblock structured meshes with around 10 million cells were used, with near-wall refinement. Based on the finite volume method, conservation of Navier–Stokes momentum in the device is described by Eq. S1 below:

$$\frac{\partial}{\partial t}(\rho\vec{V}) + \nabla\cdot(\rho\vec{V}\vec{V}) = -\nabla P + \bar{\bar{\tau}} \qquad \text{(Eq. S1)}$$

The conservation of mass is described by the continuity equation, Eq. S2:

$$\frac{\partial \rho}{\partial t} + \nabla\cdot(\rho\vec{V}) = 0 \qquad \text{(Eq. S2)}$$

ρ is the fluid density, $\vec{V}$ is the velocity vector, P is the pressure, $\bar{\bar{\tau}}$ is the stress

tensor, t is time and ∇ is the standard spatial grad operator. The physical properties of water were applied to the fluids participating in the simulation (density ρ=1000 kg·m^{-3} and dynamic viscosity μ=10^{-3} kg·m^{-1}·s^{-1}). A diffusion coefficient D=10^{-10} m^2·s^{-1} was used for the fluids in the simulations. In addition, for fluid mixing calculation, water A and B are set as 1 and 0, respectively. A second-order limiting scheme was used for solving the species diffusion. The convergence limit for mass fraction was set to 10^{-6} and the simulations were run for ≈ 2000 times steps until the flow reached the outlet.

Microfluidic device fabrication

Microfluidic device was fabricated utilizing standard soft lithography with PDMS. AutoCAD software was used to design the patterns for microchannels, which were then printed on transparent films (MicroCAD Photomask, Ltd., Suzhou, China) to form a photomask. Thereafter, the mold was constructed through one step under UV light using SU8-2050 photoresist (Microchem, MA, USA) on mask aligner (7 mW cm^{-2}, CETC, China). The mold was exposed to trimethylchlorosilane vapor for 60 min before fabrication of the microfluidic chip. Then, well-mixed PDMS pre-polymer [RTV 615 A and B (10:1, w/w)] was poured onto the mold placed in a Petri dish to yield 3×10^3 μm-thick PDMS replica. After degassing, the mold was baked at 80°C for 30 min, and the PDMS replica was peeled off the mold. Afterwards, oxygen plasma treatment was used to make the glass and PDMS surface hydrophilic. The plasma treatment provided a strong and irreversible bonding between them to avoid leakage. Finally, the device was ready to use after baking at 80℃ for 2 h.[3-5]

Operating procedure

Before operation, the microfluidic device is washed sequentially with 75% ethanol and PBS supplemented at a flow rate of 200 μL min^{-1} from Inlet 1 and Inlet 2. The cell suspension with appropriate cell density is injected by the syringe pump under optimized flow condition from corresponding Outlet 1 to Outlet 9 (Fig. S1). After cell capture, the cell medium/the medium solution of aptamer/ITF-β/Cisplatin & fresh medium are driven by the syringe pump from Inlet 1 and Inlet 2 for cell culture and aptamer labelling (1 μL min^{-1}). The capillaries (COLE-PAEMER, 2000 μm×190 μm) are connected with ordinary stainless steel tube (25 G) for introducing solution into the microfluidic chip.

The shear stress

The shear stress ($\tau_{(cell)}$) was calculated using the following equation:

$$\tau_{(cell)} = \frac{6Q\eta}{h^2 w} \qquad \text{Eq. (S3)}$$

$$Q=UA \qquad \text{Eq. (S4)}$$

Q is the volumetric flow rate, η is the dynamic viscosity, h is the channel height, w

is the width. *U* is the linear flow rate and *A* is the cross sectional area of the microchannel or microchamber.[6, 7]

Cell viability and phenotyping

MTT assay is designed to detect the cell viability. After culturing the cells with specified concentration of aptamer, the medium was removed, and the cells were incubated with MTT solution (0.5% (m/v)) for 4 h. Then the MTT solution was removed and DMSO was added allowing for vibration for 10 min, and the absorbance was measured utilizing the microplate reader at 570 nm.[8]

The PDL1 aptamer (apt-PDL1) with various concentrations, i.e., 1, 2, 5,10, 20, 50, 100, 150, 200 nM,, were used to compare the data-platform obtained in our microfluidic method to conventional methods in 96 well assay plates. The experiment was performed to validate the concentration values of each culture chamber that was predicted by simulation. SK-Hep-1 and HepG2 cell suspensions (100–200 cells μL^{-1}) in DMEM were added to each of 96 well assay plates. After 12 h the cells adhered to the plate, and the original medium was replaced with different concentration of aptamer medium.

We constructed ITF-β or Cisplatin concentration gradients by introducing ITF-β (10^5 IU mg^{-1}) or Cisplatin (50 μM) to Inlet 1 respectively and introducing PBS to Inlet 2 for profiling ITF-β-mediated or Cisplatin-mediated phenotypes.

Preparation of Apt-PDL1 and binding affinity analysis

The aptamer PDL1 (Apt-PDL1) are labeled AMCA at 3' terminal, which were synthesized by Sangon Biotech (Shanghai, China). The Apt-PDL1 sequence is 5'-TTTTTTTTTTCACTACAGAGGTTGCGTCTGTCCCACGTTGTCATGGGGGGTTGGCCTG-3'-AMCA. The DNA (100 M, 7.5 μL) was divided into 10 Eppendorf tubes to 100 μL for subsequent analysis.

To determine the variation of PD-L1 expression and binding affinity of Apt-PDL1 against cells, adhesive SK-Hep-1 cells (about 10^5 cells) were incubated with a series of concentrations of the abovementioned aptamer conjugates in 200 μL buffer (PBS with 5 mM $MgCl_2$, pH=7.4) at 37℃. The cells were washed twice with cold buffer, and they were then analyzed by microplate reader (Synergy H1, BioTek, USA). The experimental conditions were the same as those described above. The dissociation constant values (K_d) for Apt-PDL1 against cells were obtained by fitting the dependence of fluorescence intensity (Y) on the concentration of ligands (X) to the equation $Y = BmaxX/(K_d + X)$ by SigmaPlot software.[9, 10]

Concentration gradient stability of the microfluidic devices

The cell culture period usually is 3 or 4 days. Thus, to determine how robust the microfluidic system is, we generated concentration gradients for 4 days for in vitro tumor culture. First, we perfused the Aptamer (from Inlet 1) and PBS (from Inlet 2) in the microfluidic device by a syringe pump continuously. Next, we monitored the fluorescence intensity of each culture chamber every 24 hours by photographic

equipment. Finally, we investigated and compared the concentration gradients of every culture chamber in 4 days using Image-Pro1 Plus 6.0 (Media Cyternetics, Silver Spring, MD) and origin 9 (origin Inc.).

Results and Discussion

Optimization of flow rate and cell density

Cell capture rate was evaluated by comparing the number of captured cells in the chip with the number of single-cell traps. An SK-Hep-1 cell suspension was injected into the chip through corresponding outlets. Due to spatial barriers, these single-cell or single cell-clusters were intercepted and directed to parallel single-cell traps. First, the effect of flow velocity was tested (Fig. S1A). For a flow rate of 1 μL/min, the cells tended to precipitate at the chip inlet due to gravity. However, at a higher flow rate of 10 μL/min, the cells are squeezed through a 6 mm wide slit in the capture area due to high shear stress. The optimization flow rate was derived to be 3 μL/min, producing more than 90% whole capture rates for single-cell/single cell-clusters.

We finally selected the flow rate of 3 μL/min, and the total cell capture rate was as high as 99%, of which the capture rate of single cells and single cell-clusters were about 45% and 54% respectively. For optimizing the cell density, we tested the cell suspension of SK-Hep-1 with density of 1×10^4 cells /mL to 1×10^7 cells/mL (Fig. S1B). The test results showed that the higher cell density provided more favorable chance for trapping cells with respect to lower cell density. Individual cells or single cell-clusters were forced into narrow traps at higher density (1×10^7 cells/mL) because a group of cells could block the wide side temporarily. In this case, the capture efficiencies of single-cell and single cell-clusters were increased than low cell density. Thus, the cell density of 1×10^7 cells /mL was finally selected for subsequent unicellular exploration.

Supporting Figures

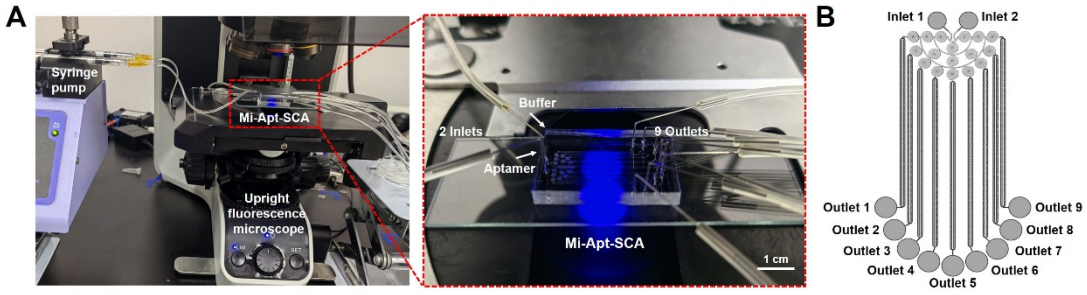

Fig. S1. (A) Photographs of the Mi-Apt-SCA system. (B) Schematic diagram of Mi-Apt-SCA chip on the top view.

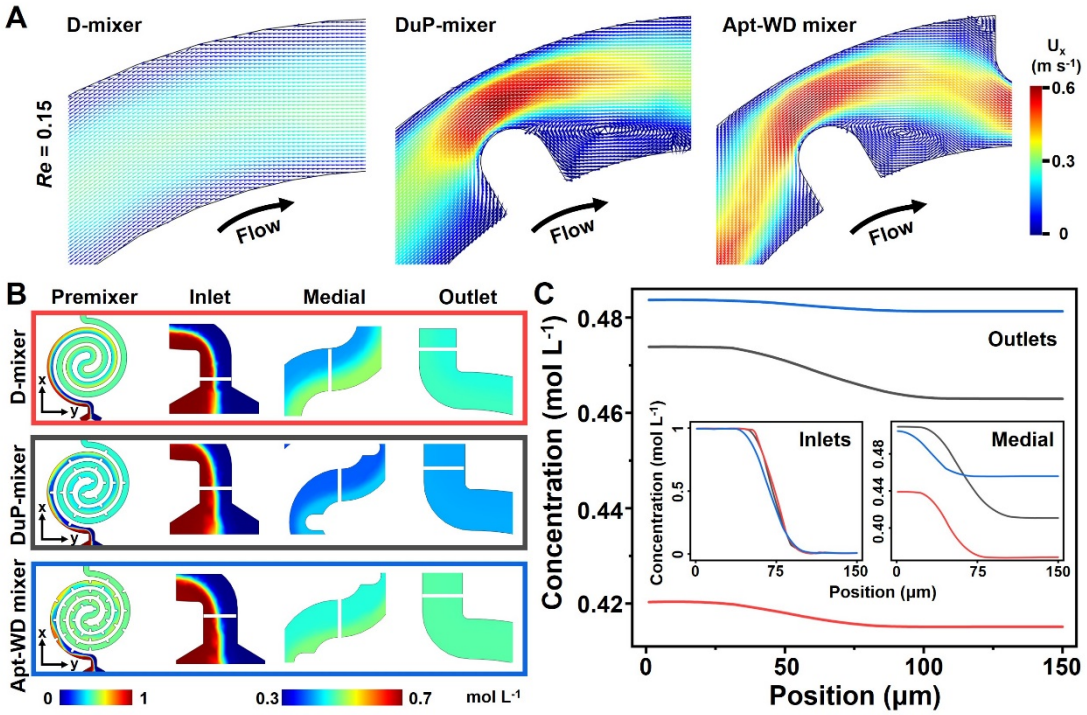

Fig. S2. (A) Representative fluid velocity field of the inertial flow (flow rate 1 μl min^{-1}, *Re* 0.42) along the D-mixer, DuP-mixer, and Apt-WD mixer. (B) Simulated images of 3 different positions of the D-mixer, DuP-mixer, and Apt-WD (flow rate 1 μl min^{-1}, *Re* 0.42). (C) The quantitative gradients characterization (C) corresponding to white straight lines positions in Fig. S2A.

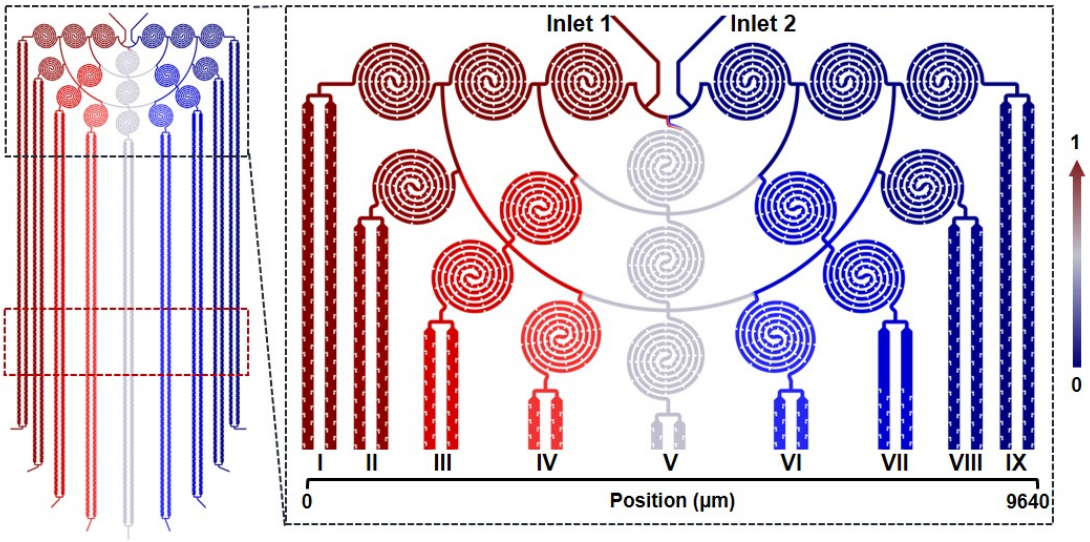

Fig. S3. The concentration simulation of the Mi-Apt-SCA system with COMSOL (flow rate 1 μL min^{-1}, *Re* 0.42).

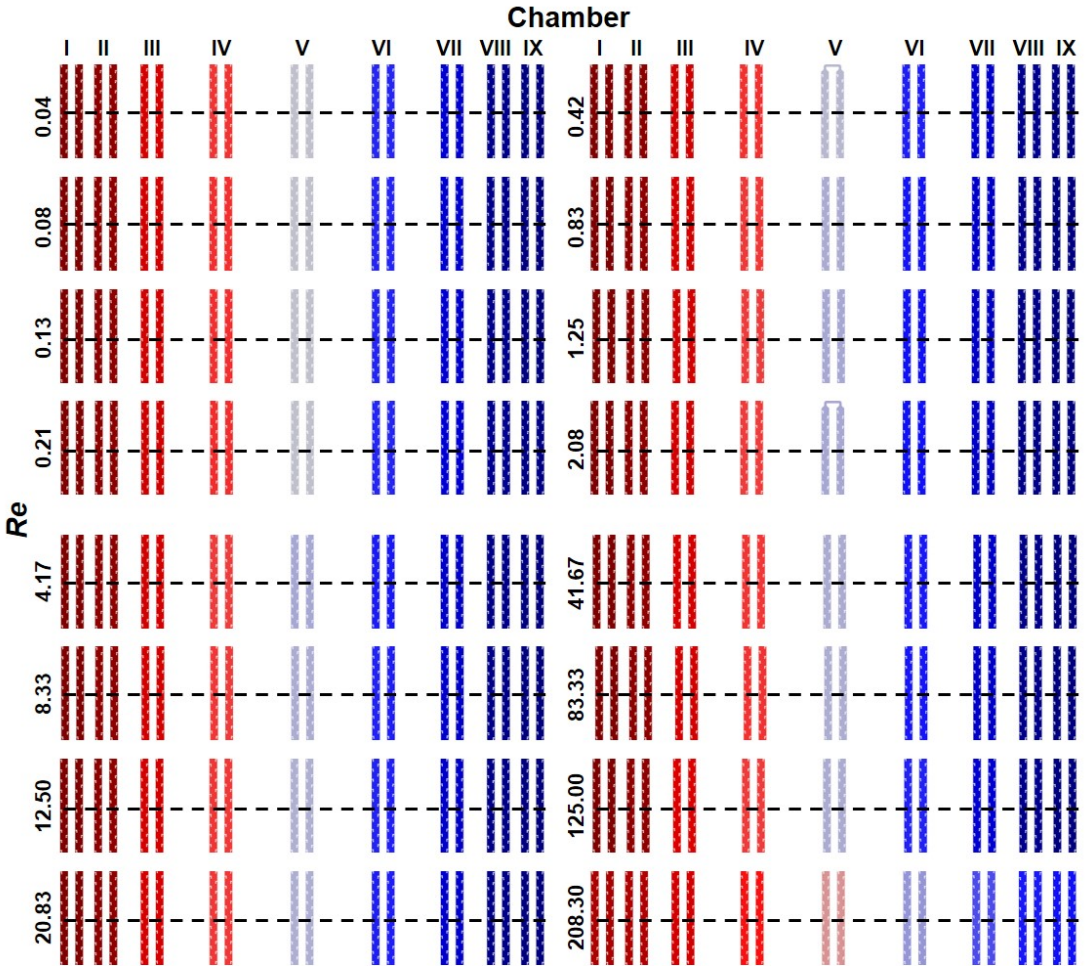

Fig. S4. The concentration simulation of the Mi-Apt-SCA with COMSOL under various flow rates of 0.1, 0.2, 0.3, 0.5, 1.0, 2.0, 3.0, 5.0, 10.0, 20.0, 30.0, 50.0, 100.0, 200.0, and 300.0 µL min^{-1} (*Re*=0.04, 0.08, 0.13, 0.21, 0.42, 0.83, 1.25, 2.08, 4.17, 8.33, 12.50, 20.83, 41.67, 83.33, 125.00, and 208.30).

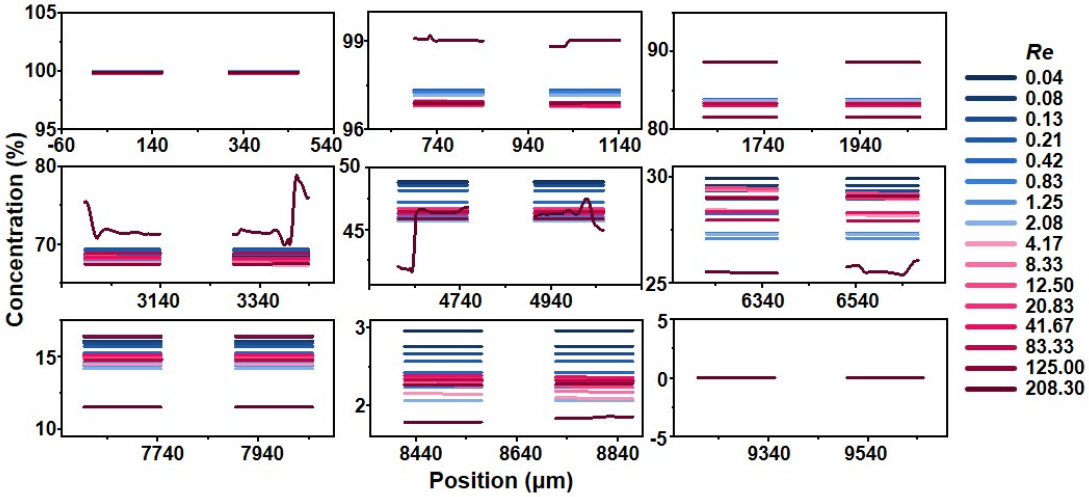

Fig. S5. Quantitative characterization gradients under various flow rates of 0.1, 0.2, 0.3, 0.5, 1.0, 2.0, 3.0, 5.0, 10.0, 20.0, 30.0, 50.0, 100.0, 200.0, and 300.0 μL min^{-1} (*Re*=0.04, 0.08, 0.13, 0.21, 0.42, 0.83, 1.25, 2.08, 4.17, 8.33, 12.50, 20.83, 41.67, 83.33, 125.00, and 208.30) corresponding to the black dot lines positions in Fig. S4.

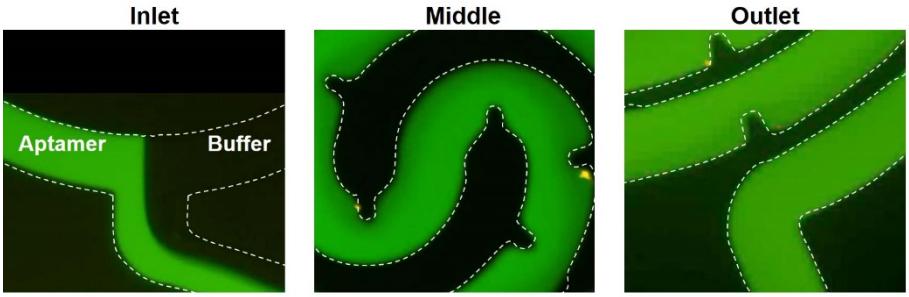

Fig. S6. Characterization of mixing performance of Apt-WD-mixer using fluorescein labeled aptamer under of 3.0 µL min^{-1} (*Re* 1.25).

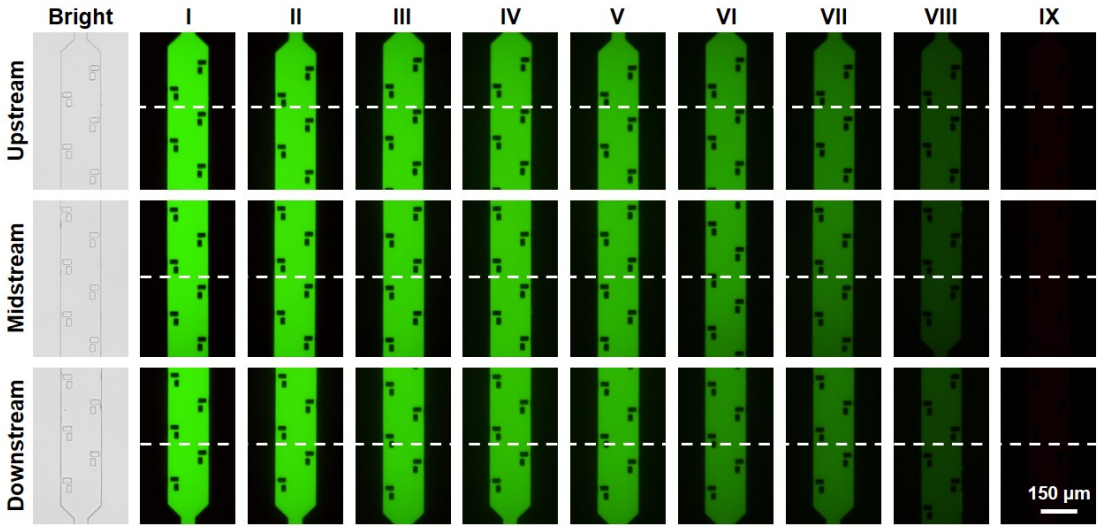

Fig. S7. Fluorescence images of fluorescein sodium distribution of the upstream, midstream and downstream in the parallel microchannels under flow rate of 1 μL min^{-1} (*Re* 0.42).

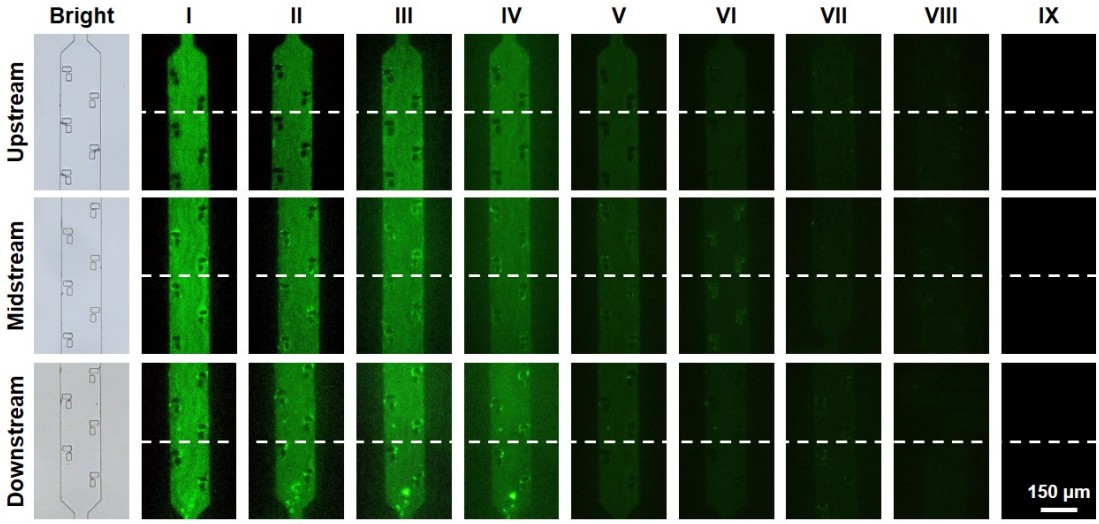

Fig. S8. Fluorescence images of 200 nm fluorescent microsphere distribution of the upstream, midstream and downstream in the parallel microchannels under flow rate of 1 μL min^{-1} (*Re* 0.42).

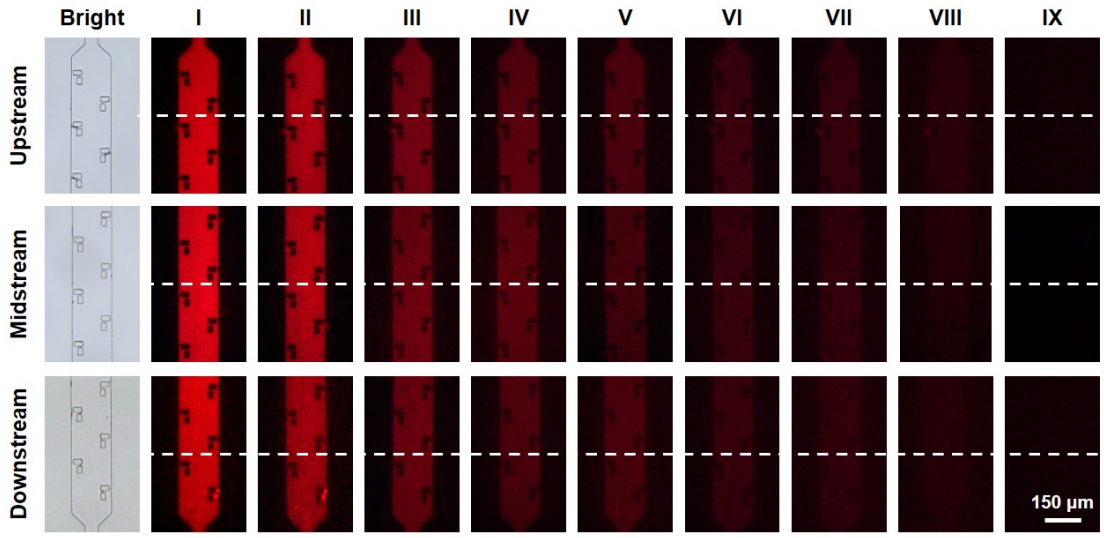

Fig. S9. Fluorescence images of 20 nm fluorescent microsphere distribution of the upstream, midstream and downstream in the parallel microchannels under flow rate of 1 μL min^{-1} (*Re* 0.42).

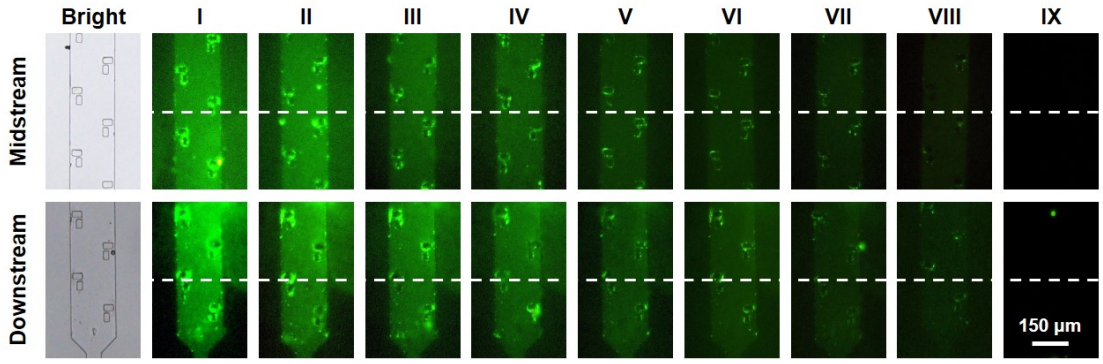

Fig. S10. Fluorescence images of apt-PDL1 distribution of the midstream and downstream in the parallel microchannels under flow rate of 1 μL min^{-1} (*Re* 0.42).

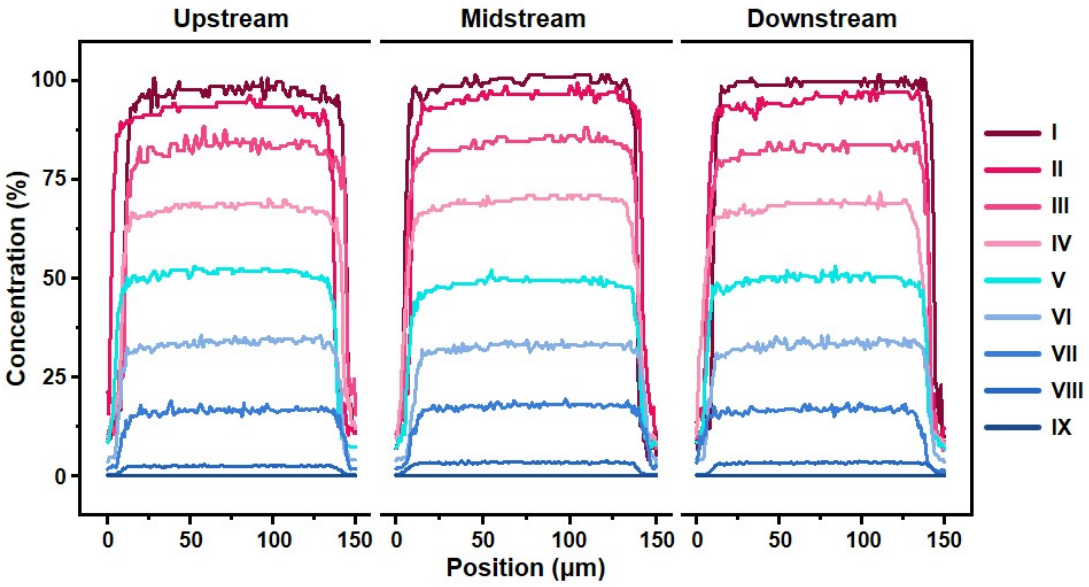

Fig. S11. Fluorescence intensity of fluorescein sodium in 3 different positions corresponding to the white dot lines positions in Fig. S7.

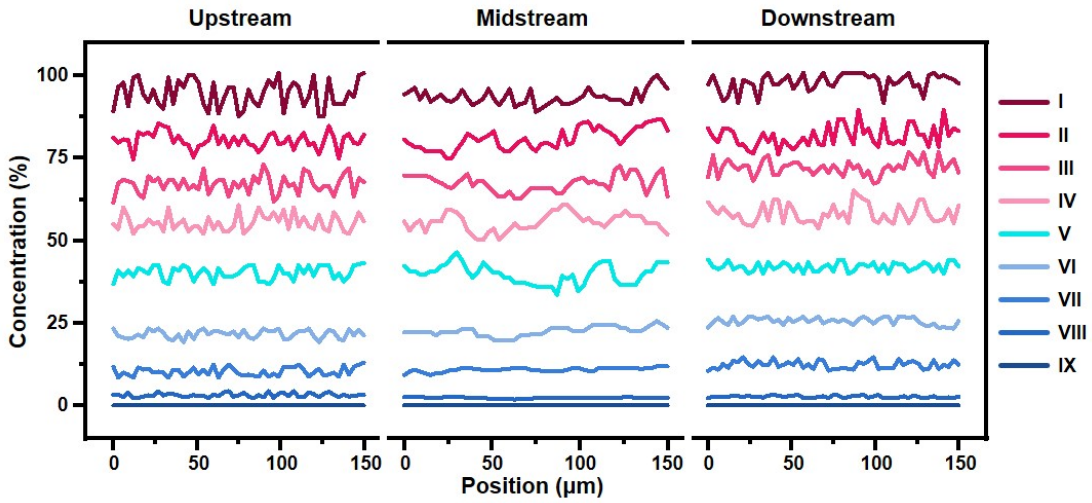

Fig. S12. Fluorescence intensity of apt-PDL1 in 3 different positions corresponding to the white dot line positions in Figs. 2A and S9.

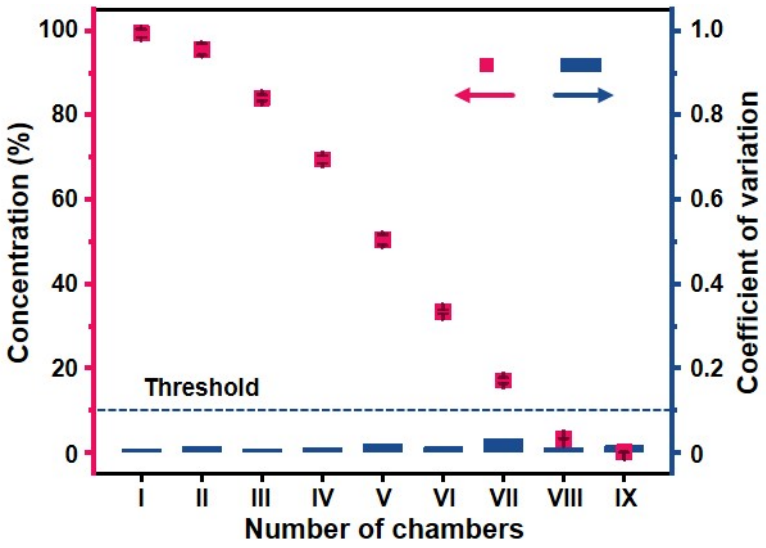

Fig. S13. The concentration gradients and CoV values of fluorescein sodium in 9 microchambers at 1 μL·min^{-1} (*Re* 0.42).

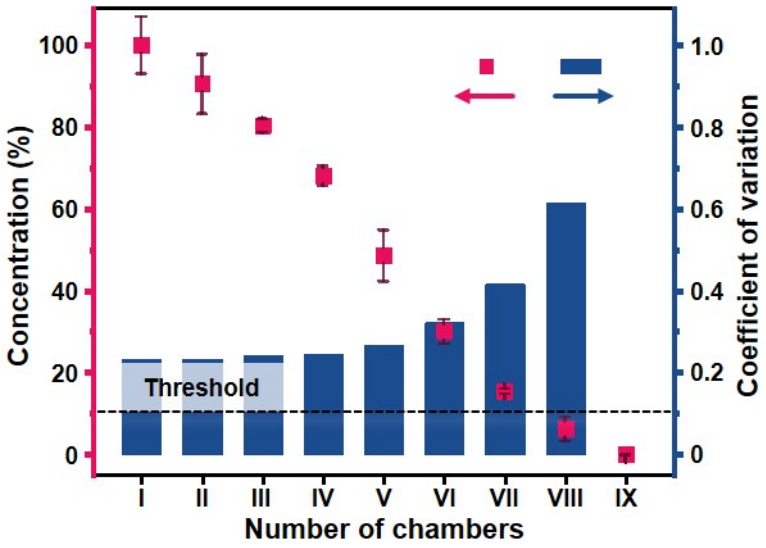

Fig. S14. The concentration gradients and CoV values of 200 nm fluorescent microsphere in 9 microchambers at 1 μL·min^{-1} (*Re* 0.42).

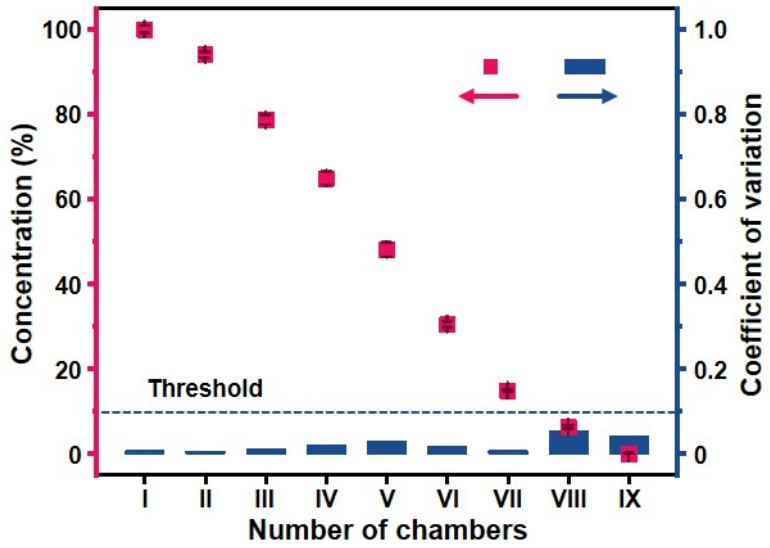

Fig. S15. The concentration gradients and CoV values of 20 nm fluorescent microsphere in 9 microchambers at 1 μL·min^{-1} (*Re* 0.42).

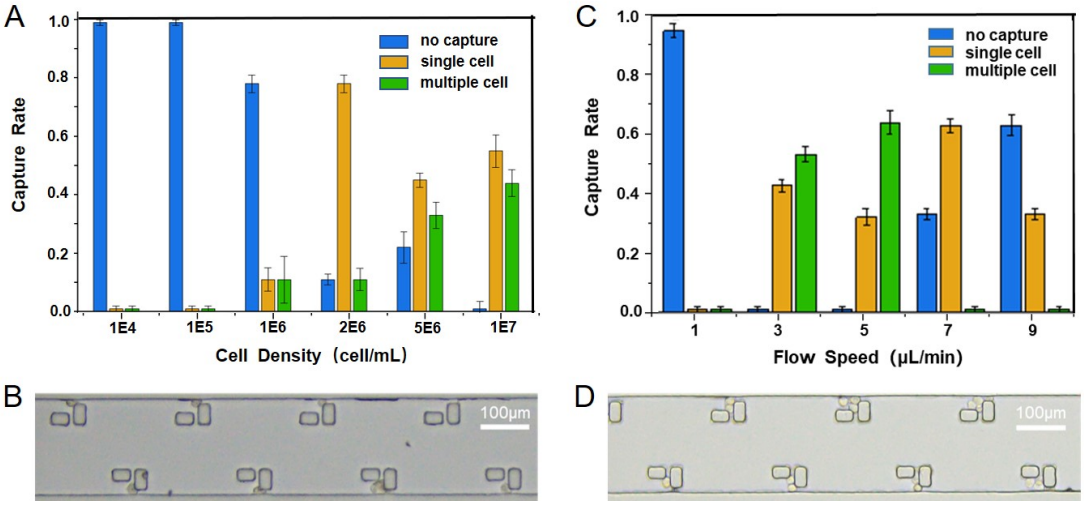

Fig. S16. Characterization of cell capture rate. Dependence of the capture rate of individual cells on the flow rates (A) and on the cell density (B). Representative captured images of individual cells (C) and single cell-clusters (D) after injection of 1×10^7 cells/mL under 3 μL/min. The error bars show the standard deviation of three replicates.

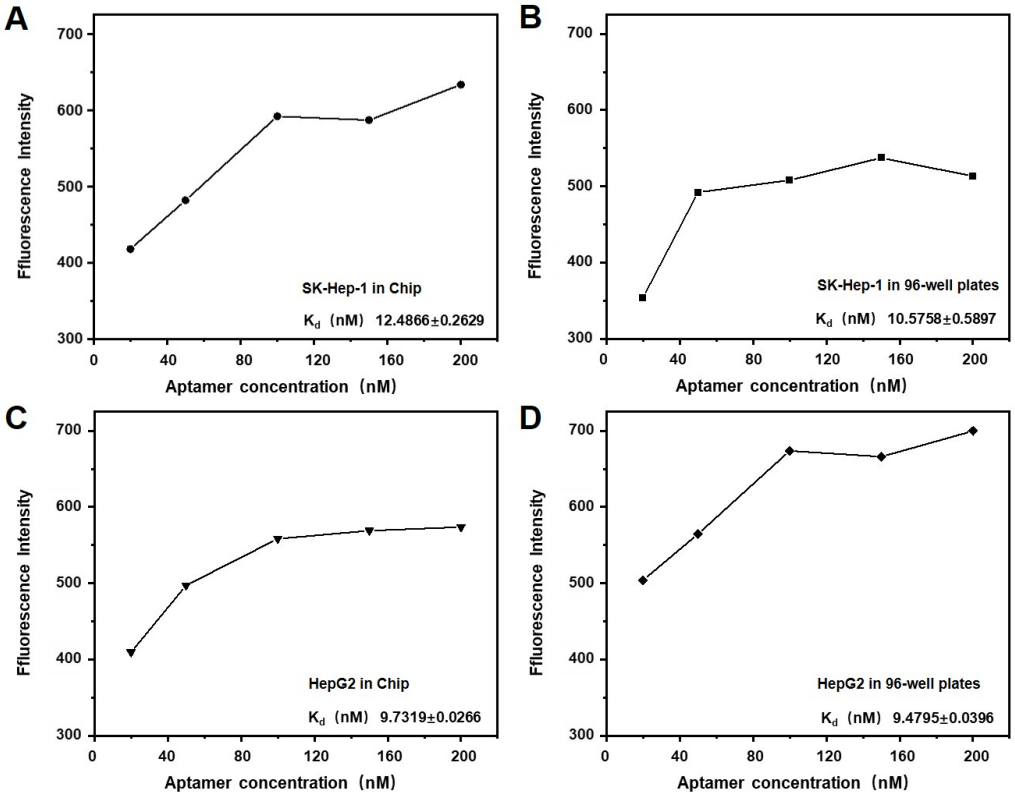

Fig. S17. The evaluation of the dissociation constants of Apt-PDL1 to SK-Hep-1 and HepG2 cells in the chip system and 96-well plates.

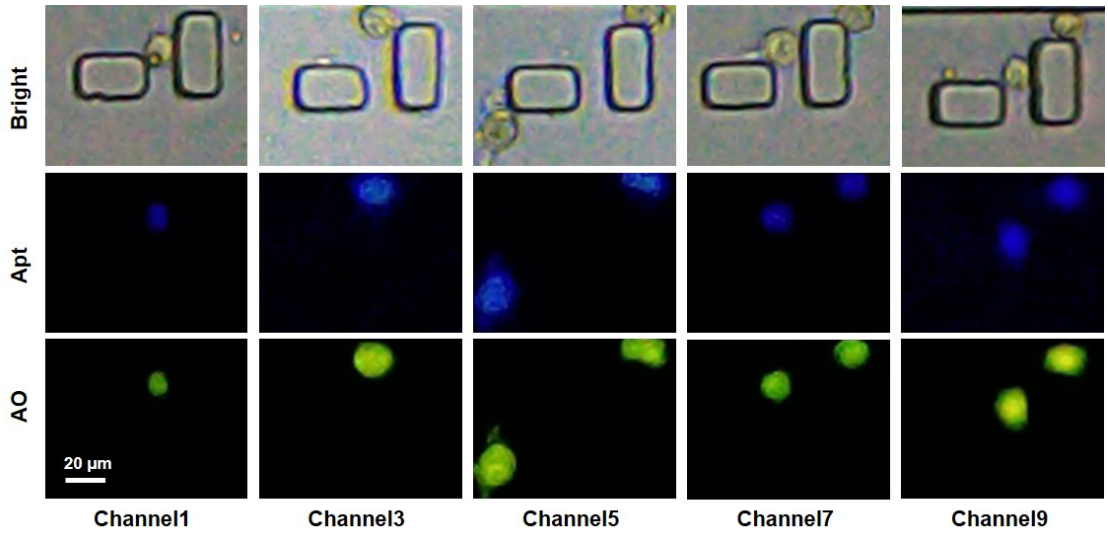

Fig. S18. Images of the HepG2 cells treated with various concentrations of Apt-PDL1.

Table S1. The comparisons of the present method with other works reported concentration gradient dilution.

Method	Theory	Flow condition	Concentration gradient	Ref.
CD shaped mixer	Secondary flows Centripetal forces	5 μl min^{-1}	Different linear concentrations gradients	Angew. Chem. Int. Ed. (2021)
D-S chip	Parallel brancher	40 μl min^{-1}	0, 25%, 50%, 75%, 100%	Chem. Sci. (2020)
μMHG-CGG mixer	Laminar flow Diffusion effects	NA	0%, 25%, 50%, 75%, 100%	Anal. Chem. (2020)
Apt-WD-mixer	Dean vortex Fluid disturbance	3 μl min^{-1}	0, 3%, 16.8%, 25.9%, 50%, 64.6%, 83.2%, 96.9%, 100%	This work

References

1. S. F. Shen, F. J. Zhang, S. T. Wang, J. R. Wang, D. D. Long, D. F. Wang and Y. B. Niu, *Sens. Actuator B-Chem.*, 2019, **287**, 320-328.
2. X. Wei, D.-H. Zheng, Y. Cai, R. Jiang, M.-L. Chen, T. Yang, Z.-R. Xu, Y.-L. Yu and J.-H. Wang, *Anal. Chem.*, 2018, **90**, 14543-14550.
3. O. Mitxelena-Iribarren, J. Zabalo, S. Arana and M. Mujika, *Biosens. Bioelectron.*, 2019, **123**, 237-243.
4. S. F. Shen, C. Tian, T. B. Li, J. Xu, S. W. Chen, Q. Tu, M. S. Yuan, W. M. Liu and J. Y. Wang, *Lab Chip*, 2017, **17**, 3578-3591.
5. B. Zheng, J. D. Tice, L. S. Roach and R. F. Ismagilov, *Angew. Chem.-Int. Edit.*, 2004, **43**, 2508-2511.
6. Y. Lu, W. C. de Vries, N. J. Overeem, X. X. Duan, H. X. Zhang, H. Zhang, W. Pang, B. J. Ravoo and J. Huskens, *Angew. Chem.-Int. Edit.*, 2019, **58**, 159-163.
7. L. Wang, W. M. Liu, Y. L. Wang, J. C. Wang, Q. Tu, R. Liu and J. Y. Wang, *Lab Chip*, 2013, **13**, 695-705.
8. H. Wang, B. B. Chen, M. He, X. X. Yu and B. Hu, *Sci Rep*, 2017, **7**, 8.
9. Y. Song, Y. Shi, M. Huang, W. Wang, Y. Wang, J. Cheng, Z. Lei, Z. Zhu and C. Yang, *Angew. Chem.-Int. Edit.*, 2019, **58**, 2236-2240.
10. E. Sinkala, E. Sollier-Christen, C. Renier, E. Rosàs-Canyelles, J. Che, K. Heirich, T. A. Duncombe, J. Vlassakis, K. A. Yamauchi, H. Huang, S. S. Jeffrey and A. E. Herr, *Nature Communications*, 2017, **8**, 14622.